Titanium Oxide Complexes with Dinitrogen. Formation and Characterization of the Side-On and End-On Bonded Titanium Oxide-Dinitrogen Complexes in Solid Neon

ARTICLE *in* THE JOURNAL OF PHYSICAL CHEMISTRY A · JUNE 2011

Impact Factor: 2.69 · DOI: 10.1021/jp203352e · Source: PubMed

7 AUTHORS, INCLUDING:

Mingfei Zhou
Fudan University
259 PUBLICATIONS **5,074** CITATIONS
SEE PROFILE

Zhen Hua Li
Fudan University
77 PUBLICATIONS **1,160** CITATIONS
SEE PROFILE

Xuming Zheng
Zhejiang Sci-Tech University
109 PUBLICATIONS **1,256** CITATIONS
SEE PROFILE

Kangnian Fan
Fudan University
181 PUBLICATIONS **3,743** CITATIONS
SEE PROFILE

THE JOURNAL OF PHYSICAL CHEMISTRY A

ARTICLE

pubs.acs.org/JPCA

Titanium Oxide Complexes with Dinitrogen. Formation and Characterization of the Side-On and End-On Bonded Titanium Oxide−Dinitrogen Complexes in Solid Neon

Mingfei Zhou,*[,†] Jia Zhuang,[†] Zijian Zhou,[‡] Zhen Hua Li,*[,†] Yanying Zhao,[‡] Xuming Zheng,[‡] and Kangnian Fan[†]

[†]Department of Chemistry, Shanghai Key Laboratory of Molecular Catalysts and Innovative Materials, Fudan University, Shanghai 200433, China

[‡]Department of Chemistry, Zhejiang Sci-Tech University, Hangzhou, China

ABSTRACT: The reactions of titanium oxide molecules with dinitrogen have been studied by matrix isolation infrared spectroscopy. The titanium monoxide molecule reacts with dinitrogen to form the $TiO(N_2)_x$ (x = 1−4) complexes spontaneously on annealing in solid neon. The $TiO(\eta^1\text{-NN})$ complex is end-on bonded and was predicted to have a $^3A''$ ground state arising from the $^3\Delta$ ground state of TiO. Argon doping experiments indicate that $TiO(\eta^1\text{-NN})$ is able to form complexes with one or more argon atoms. Argon atom coordination induces a large red-shift of the N−N stretching frequency. The $TiO(\eta^2\text{-}N_2)_2$ complex was characterized to have C_{2v} symmetry, in which both the N_2 ligands are side-on bonded to the titanium metal center. The tridinitrogen complex $TiO(\eta^1\text{-NN})_3$ most likely has C_{3v} symmetry with three end-on bonded N_2 ligands. The $TiO(\eta^1\text{-NN})_4$ complex was determined to have a C_{4v} structure with four equivalent end-on bonded N_2 ligands. In addition, evidence is also presented for the formation of the $TiO_2(\eta^1\text{-NN})_x$ (x = 1−4) complexes, which were predicted to be end-on bonded.

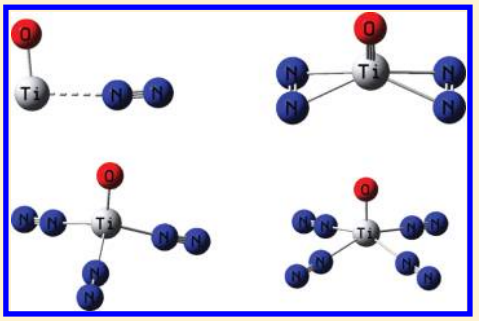

INTRODUCTION

Catalytic converting the inert molecular nitrogen into ammonia is one of the most challenging problems in small molecule activation.[1] Coordination of N_2 to transition metal centers is proposed to be the initial step of the complex sequential chemical activation of dinitrogen. Understanding the coordination of dinitrogen on transition metal centers is important in understanding catalytic dinitrogen fixation and activation. Since the first discovery of a dinitrogen complex in 1965,[2] a large number of transition metal−dinitrogen complexes have been synthesized. The structures, binding modes, and reactivity patterns of transition metal dinitrogen complexes have been extensively studied.[3−9]

Dinitrogen fixation and activation by bare metal atoms, small clusters, and simple oxide molecules serves as models in understanding the structure and bonding of larger dinitrogen complexes and clusters with various other ligands.[10] Matrix isolation studies on the reactions of bare transition metal atoms with dinitrogen indicate the formation of the end-on bonded dinitrogen complexes.[11−18] Experiments with laser-ablated metal atoms also gave evidence for the formation of side-on bonded complexes, presumably from the excited state metal atom reactions.[11,12] Some transition metal dimers are more reactive than the metal atoms toward dinitrogen.[19−21] It was found that the Sc_2 and Ti_2 dimers reacted spontaneously with dinitrogen to form the cyclic Sc_2N_2 and Ti_2N_2 compounds in which the N−N triple bond is completely cleaved.[20,21] The reactions of transition metal oxide molecules with N_2 in solid argon have also been reported. The results showed that transition metal monoxides such as ScO, TiO, MnO, and FeO and dioxides, including TaO_2 and CrO_2, are able to react with dinitrogen in forming dinitrogen complexes in solid argon.[22−28] Both the side-on and end-on coordination modes were observed, which were found to be photointercovertable in selected systems. In this paper, the reactions of titanium monoxide and dioxide molecules with dinitrogen were reinvestigated using the more inert neon matrix to minimize the matrix effect. Previous studies indicate that polar species such as transition metal oxides may be chemically coordinated by noble gas atom(s) and cannot be regarded as isolated species in heavier noble gas matrixes.[29,30] We will show that there is a large frequency difference for the $TiO(\eta^1\text{-NN})$ complex in solid argon and neon. In addition, high complexes with up to four coordinated dinitrogen ligands were formed in solid neon.

EXPERIMENTAL AND COMPUTATIONAL METHODS

The titanium oxide-dinitrogen complexes were prepared from the reactions of laser-evaporated titanium monoxide molecules with dinitrogen in solid neon and were detected by infrared absorption spectroscopy. The experimental setup for pulsed laser

Received: April 11, 2011
Revised: May 9, 2011
Published: May 23, 2011

evaporation and matrix isolation Fourier transform infrared (FTIR) spectroscopic investigation has been described in detail previously.[31] Briefly, the 1064 nm Nd:YAG laser fundamental (Continuum, Minilite II, 10 Hz repetition rate) was focused onto a rotating bulk TiO_2 target, which was prepared by sintered metal oxide powder. The laser-evaporated oxide species were codeposited with dinitrogen in excess neon onto a CsI window cooled normally to 4 K by means of a closed-cycle helium refrigerator. In general, the matrix samples were deposited for 30 min at a rate of approximately 4 mmol/h with 4−6 mJ/pulse evaporation laser energy. The N_2/Ne samples were prepared in a stainless steel vacuum line using standard manometric technique. N_2 (Shanghai BOC, 99.95%) and isotopic-labeled $^{15}N_2$ (ISOTEC, 99%) samples were used without further purification. The scrambled $^{14}N_2 + {}^{14}N^{15}N + {}^{15}N_2$ (1:2:1) mixture was prepared via Tesla coil discharge of the mixed $^{14}N_2 + {}^{15}N_2$ (1:1) sample. The infrared absorption spectra of the resulting samples were recorded on a Bruker Vertex 80 V spectrometer at 0.5 cm^{-1} resolution between 4000 and 450 cm^{-1} using a liquid nitrogen cooled mercury cadmium telluride (MCT) detector. After the infrared spectrum of the initial deposition had been recorded, the samples were warmed up to a certain temperature, quickly recooled and more spectra were taken.

Quantum chemical calculations were performed to determine the molecular structures and to support the assignment of vibrational frequencies of the observed reaction products. Geometry optimization and harmonic vibrational frequency analysis were performed with the hybrid B3LYP and the double-hybrid mPW2PLYP density functional theory (DFT) method in combination with the 6-311+G(d) basis set.[32−34] The B3LYP functional is the most popular density functional methods and can provide reliable predictions on the structures and vibrational frequencies of early transition metal-containing compounds.[35] Recent benchmark calculations indicate that the double-hybrid DFT methods show superior performance compared to common DFT methods in many applications.[36] Transition state optimizations were done with the synchronous transit-guided quasi-Newton (STQN) method and were verified through intrinsic reaction coordinate (IRC) calculations.[37] It should be noted here that the singlet wave functions of most $TiO(N_2)_n$ (n = 1−4) complexes have RHF-UHF instability and were optimized with the "stable" keyword as implemented in the Gaussian 09 program. All these calculations were performed by using the Gaussian 09 program.[38]

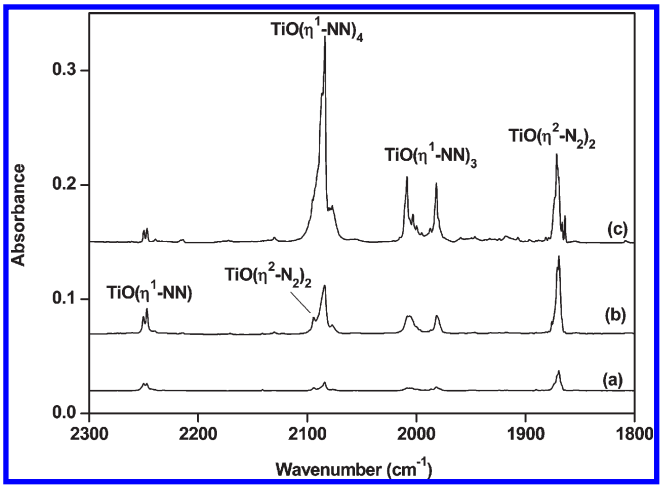

Figure 1. Infrared spectra in the 2300−1800 cm^{-1} region from codeposition of laser-evaporated titanium oxides with 0.05% N_2 in neon: (a) 30 min of sample deposition at 4 K, (b) after 10 K annealing, and (c) after 12 K annealing.

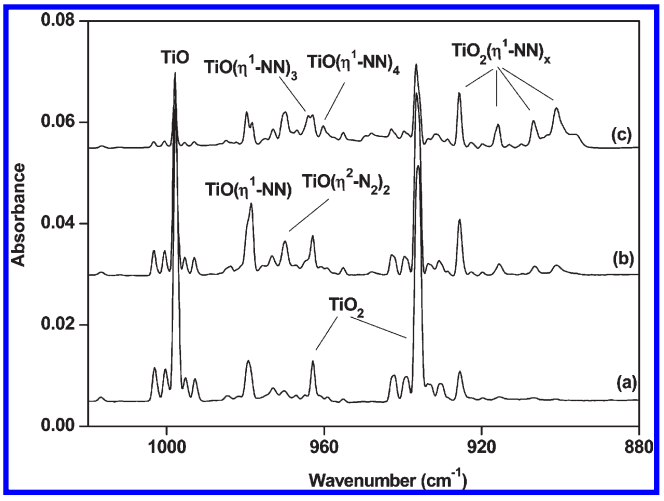

Figure 2. Infrared spectra in the 1020−880 cm^{-1} region from codeposition of laser-evaporated titanium oxides with 0.05% N_2 in neon: (a) 30 min of sample deposition at 4 K, (b) after 10 K annealing, and (c) after 12 K annealing.

RESULTS AND DISCUSSIONS

Infrared Spectra. The titanium oxide molecules were prepared by pulsed laser evaporation of bulk TiO_2 target. Pulsed laser evaporation of bulk TiO_2 target under controlled laser energy followed by condensation with pure neon formed only the TiO (997.9 cm^{-1} for ^{48}TiO) and TiO_2 (ν_3: 936.7 cm^{-1} and ν_1: 962.9 cm^{-1} for $^{48}TiO_2$) molecules.[39] No other oxide species were observed.[39,40] Experiments were performed using the N_2/Ne samples as reagent gas. A series of experiments was done with different N_2 concentrations ranging from 0.02 to 0.1% in neon. The spectra in the N−N stretching and Ti═O stretching vibrational frequency regions from codeposition of laser evaporated titanium oxides with 0.05% N_2 in neon are shown in Figures 1 and 2, respectively. After 30 min of sample deposition at 4 K, strong TiO and TiO_2 absorptions were observed. Product absorptions were produced upon sample annealing at the expense of the TiO and TiO_2 absorptions. These product absorptions can be classified into several groups on the basis of the changes of the intensities as a function of annealing. The band positions of the product absorptions are listed in Table 1.

Experiments were also repeated using the isotopic-labeled $^{15}N_2$ sample and the $^{14}N_2 + {}^{15}N_2$ and $^{14}N_2 + {}^{14}N^{15}N + {}^{15}N_2$ mixtures. In the experiment with $^{15}N_2$, all the absorptions in the N−N stretching frequency region are shifted, whereas the absorptions in the Ti═O stretching frequency region show no shift. The spectra in the N−N stretching frequency region with the $^{14}N_2 + {}^{15}N_2$ and $^{14}N_2 + {}^{14}N^{15}N + {}^{15}N_2$ mixtures are shown in Figures 3 and 4, respectively, with the isotopic counterparts also summarized in Table 1.

Complementary experiments were performed with 0.2% to 1.0% argon doped into the neon matrix gas. Figure 5 shows the spectra in the N−N stretching frequency region from codeposition of laser-evaporated titanium oxide molecules with 0.05% N_2

dx.doi.org/10.1021/jp203352e |J. Phys. Chem. A 2011, 115, 6551–6558

Table 1. Infrared Absorptions (cm^{-1}) from Codeposition of Laser-Evaporated Titanium Oxide Molecules with Dinitrogen in Solid Neon

$^{14}N_2$	$^{15}N_2$	$^{14}N_2 + {}^{15}N_2$	assignment
2247.1	2172.8	2247.1, 2172.8	TiO(η^1-NN) NN str.
979.7	979.7		TiO(η^1-NN) TiO str.
1901.9	1839.1	1901.9, 1839.1	TiO(η^1-NN)$(Ar)_x$ NN str.
959.4	959.4		TiO(η^1-NN)$(Ar)_x$ TiO str.
2094.2	2024.7	2094.2, 2064.0, 2024.7	TiO(η^2-N_2)$_2$ sym. NN str.
1871.4	1809.4	1871.4, 1835.1, 1809.4	TiO(η^2-N_2)$_2$ antisym. NN str.
969.9	969.9		TiO(η^2-N_2)$_2$ TiO str.
2008.6	1942.6		TiO(η^1-NN)$_3$ NN str.
1981.7	1916.0		TiO(η^1-NN)$_3$ NN str.
964.0	964.0		TiO(η^1-NN)$_3$ TiO str.
2084.0	2015.2	2084.0, 2056.0, 2040.7, 2024.9, 2015.2	TiO(η^1-NN)$_4$ NN str.
960.2	960.2		TiO(η^1-NN)$_4$ TiO str.
955.2	955.2		TiO_2(η^1-NN) TiO_2 sym. str.
925.5	925.5		TiO_2(η^1-NN) TiO_2 antisym. str.
915.8	915.8		TiO_2(η^1-NN)$_2$ TiO_2 antisym. str.
906.8	906.8		TiO_2(η^1-NN)$_3$ TiO_2 antisym. str.
901.0	901.0		TiO_2(η^1-NN)$_4$ TiO_2 antisym. str.

doped with 1.0% Ar in neon. The relative intensities of the product absorptions changed significantly upon argon doping. In addition, new absorptions were observed to evolve upon sample annealing to different temperatures. Similar experiment with the $^{14}N_2 + {}^{15}N_2$ mixed sample was also done and the spectra in the N−N stretching frequency region are illustrated in Figure 6.

TiO(η^1-NN). The 2247.1 and 978.6 cm^{-1} absorptions increased together on low temperature (10 K) sample annealing but decreased on high temperature (12 K) annealing. The 2247.1 cm^{-1} absorption shifted to 2172.8 cm^{-1} when the $^{15}N_2$/Ne sample was used. The resulting $^{14}N/^{15}N$ isotopic frequency ratio (1.0342) and band position indicate that this absorption is due to the N−N stretching vibration of an end-on bond N_2 ligand. No intermediate absorption was observed in the experiment with the $^{14}N_2 + {}^{15}N_2$ sample (Figure 3), indicating that only one N_2 ligand is involved in this mode. The 978.6 cm^{-1} absorption lies in the region for a terminal Ti═O stretching vibration. The band position is 19.3 cm^{-1} red-shifted from the vibration of TiO in solid neon.[39] Accordingly, the 2247.1 and 978.6 cm^{-1} absorptions are assigned to the N−N and Ti═O stretching vibrations of the TiO(η^1-NN) complex in solid neon. The TiO(η^1-NN) complex was previously produced via the reactions of TiO with N_2 or titanium atom with N_2O in solid argon.[26] The N−N stretching and Ti═O stretching modes were observed at 1901.3 and 954.5 cm^{-1} in solid argon, which are red-shifted by 345.8 and 24.1 cm^{-1} from the neon matrix values. Such large shifts suggest that there is strong interaction between TiO(η^1-NN) and the matrix atoms. As has been discussed,[26] the TiO(η^1-NN) complex was predicted to be able to coordinate argon atoms in forming argon complex, in which argon atom serves as an electron donor. Argon atom coordination enhanced the back-donation interaction between Ti and N_2 and significantly elongated

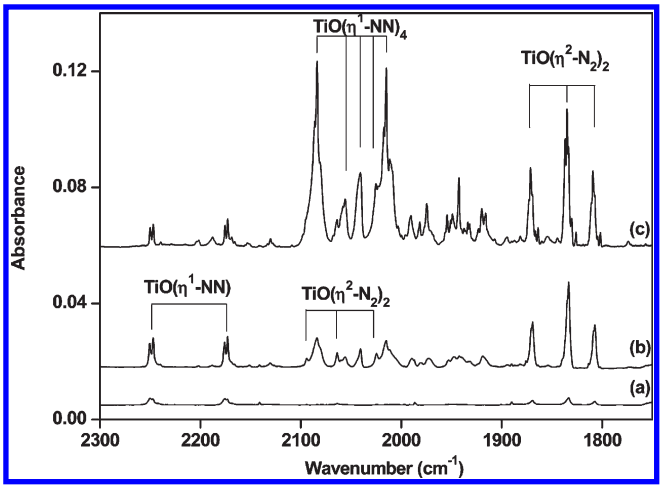

Figure 3. Infrared spectra in the 2300−1750 cm^{-1} region from codeposition of laser-evaporated titanium oxides with 0.05% $^{14}N_2$ + 0.05% $^{15}N_2$ in neon: (a) 30 min of sample deposition at 4 K, (b) after 10 K annealing, and (c) after 12 K annealing.

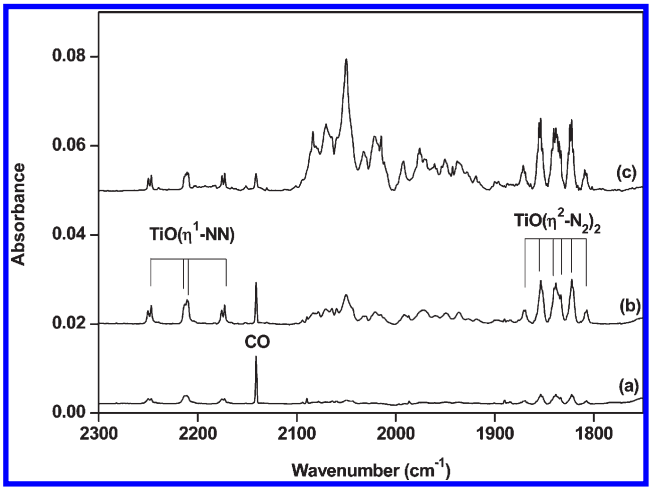

Figure 4. Infrared spectra in the 2300−1750 cm^{-1} region from codeposition of laser-evaporated titanium oxides with 0.1% ($^{14}N_2$ + $^{14}N^{15}N$ + $^{15}N_2$) in neon: (a) 30 min of sample deposition at 4 K, (b) after 10 K annealing, and (c) after 12 K annealing.

the N−N bond length and, as a result, induced a large red-shift of the N−N stretching vibrational frequency. In the argon doping experiment, a sharp absorption at 1901.9 cm^{-1} was produced on annealing. This absorption is assigned to the N−N stretching vibration of the TiO(η^1-NN)$(Ar)_x$ complex in solid neon.

Density functional calculations predicted that the TiO(η^1-NN) complex has a $^3A''$ ground state with C_s symmetry (Figure 7). The harmonic N−N stretching vibration of the $^3A''$ ground state TiO(η^1-NN) complex was calculated to be 2339.4 cm^{-1} at the mPW2PLYP/6-311+G(d) level, in good agreement with the observed value. However, the calculations at the B3LYP/6-311+G(d) level gave a value of 2196.6 cm^{-1}, about 50.5 cm^{-1} lower than the observed value. Apparently, the N−N stretching frequency is underestimated with the B3LYP functional.

TiO(η^2-N_2)$_2$. The 2094.2, 1871.4, and 969.9 cm^{-1} absorptions markedly increased together on annealing after the TiO(η^1-NN)

dx.doi.org/10.1021/jp203352e |J. Phys. Chem. A 2011, 115, 6551–6558

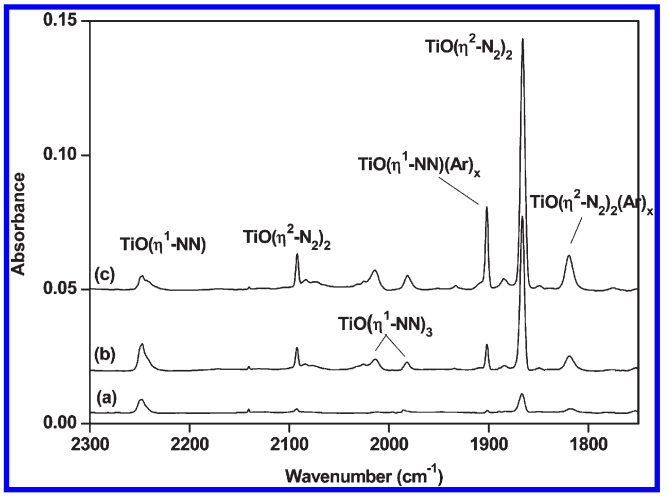

Figure 5. Infrared spectra in the 2300−1750 cm^{-1} region from codeposition of laser-evaporated titanium oxides with 0.05% N_2+ 1.0% Ar in neon: (a) 30 min of sample deposition at 4 K, (b) after 10 K annealing, and (c) after 12 K annealing.

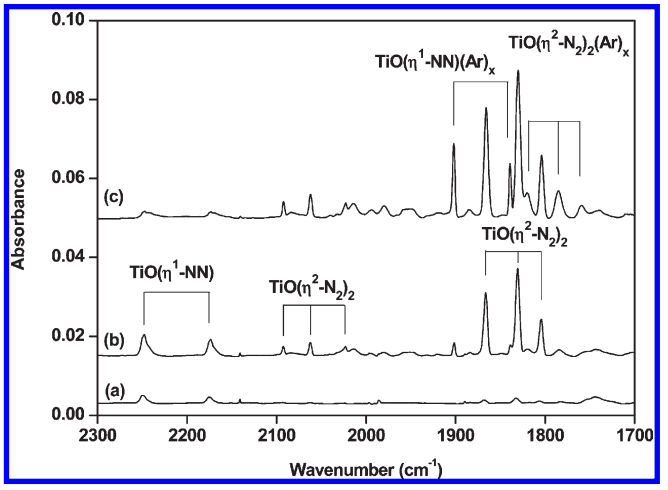

Figure 6. Infrared spectra in the 2300−1700 cm^{-1} region from codeposition of laser-evaporated titanium oxides with 0.1% ($^{14}N_2 + {}^{15}N_2$) + 1.0% Ar in neon: (a) 30 min of sample deposition at 4 K, (b) after 10 K annealing, and (c) after 12 K annealing.

absorptions. The 969.9 cm^{-1} absorption showed no shift with $^{15}N_2$. The band position is 28.0 cm^{-1} red-shifted from the TiO stretching vibration in solid neon. The band positions and nitrogen isotopic shifts indicate that both the 2094.2 and 1871.4 cm^{-1} absorptions are due to N−N stretching vibrations. In the experiments with the mixed $^{14}N_2 + {}^{15}N_2$ sample, each mode splits into a triplet (Figure 3), indicating that two equivalent N_2 subunits are involved in these two modes. Although the isotopic structure in the experiment with scrambled $^{14}N_2 + {}^{14}N^{15}N + {}^{15}N_2$ sample is too weak to be resolved for the upper mode due to isotopic dilution, a sextet can be clearly resolved for the low mode, which indicates that four equivalent N atoms are involved. Accordingly, we assign the 2094.2, 1871.4, and 969.9 cm^{-1} absorptions to different vibrational modes of the TiO(η^2-N_2)$_2$ complex with two equivalent side-on bonded N_2 ligands. The absorption at 1819.8 cm^{-1} observed in the

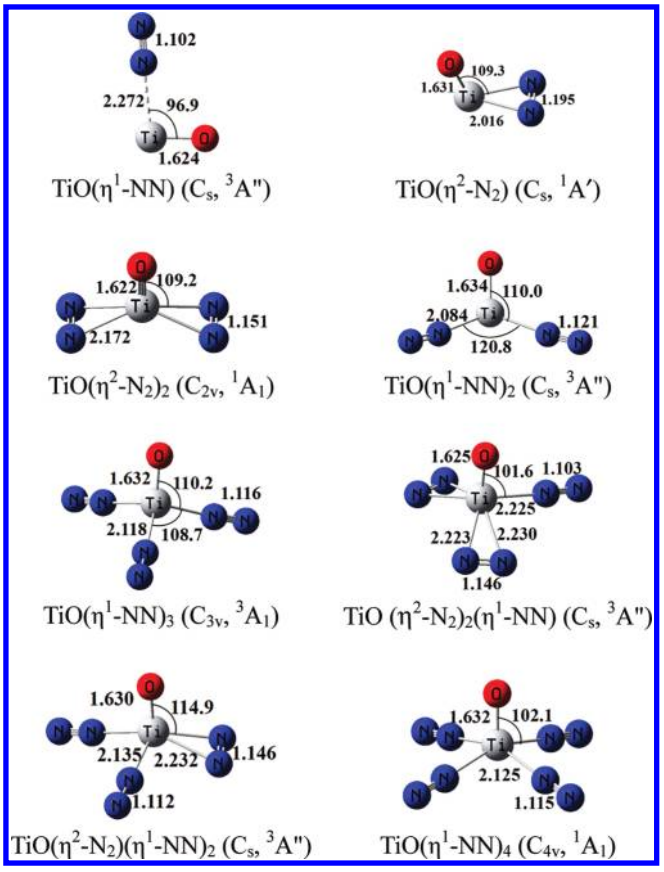

Figure 7. Structures (bond lengths in Å and bond angles in degrees) of $TiO(N_2)_n$ (n = 1−4) optimized at the mPW2PLYP/6-311+G(d) level.

experiment with argon doping is due to argon coordinated TiO-(η^2-N_2)$_2$(Ar)$_x$ complex.

Theoretical calculations were performed to support the assignment. Calculations were performed on the singlet and triplet spin states of $TiO(N_2)_2$ in both the side-on and end-on bonded structures, and the results are summarized in Figure 7. At the B3LYP level of theory, the most stable structure of $TiO(N_2)_2$ was predicted to be an $^3A''$ triplet state with two end-on bonded N_2 ligands. However, at the mPW2PLYP level of theory, a singlet state with two side-on bonded N_2 ligands was predicted to be the ground state, which lies slightly lower in energy than the $^3A''$ state end-on bonded structure. The vibrational frequencies predicted for the singlet state side-on bonded TiO(η^2-N_2)$_2$ complex are in reasonable agreement with the experimental values. It should be pointed out that the mPW2PLYP calculations significantly underestimated the IR intensity of the antisymmetric N−N stretching vibration.

TiO(η^1-NN)$_3$. The 2008.6, 1981.7, and 964.0 cm^{-1} absorptions formed and increased together on annealing after the TiO(η^2-N_2)$_2$ absorptions and are assigned to the N−N and Ti═O stretching modes of the $TiO(N_2)_3$ complex. The nitrogen isotopic splitting in the mixed $^{14}N_2 + {}^{15}N_2$ and $^{14}N_2 + {}^{14}N^{15}N + {}^{15}N_2$ experiments cannot be well resolved due to isotopic dilution. The structure cannot clearly be determined based on the experimental observations. Calculations were performed on the singlet and triplet spin states of $TiO(N_2)_3$ with various structures, and the results are summarized in Figure 7. At both levels of theory, the most stable structure of $TiO(N_2)_3$ was predicted to be an $^3A_1$ state with C_{3v} symmetry involving three

Table 2. Relative Energy (kcal/mol), Harmonic Vibrational Frequencies (cm^{-1}), and Intensities (in Parentheses in km/mol) of the $TiO(N_2)_x$ ($x = 1-4$) Complexes Calculated at the mPW2PLYP/6-311+G(d) Level

	relative energy	ν_{TiO}	ν_{NN}	ν_{NN}	ν_{NN}
N_2			2376.0		
TiO ($^3\Delta$)		1034.3 (161)			
TiO(η^1-NN) (^{3}A″)	0.0	1015.4 (174)	2339.4 (78)		
TiO(η^2-N_2) ($^1A_1$)	0.5	1000.1 (155)	1724.6 (279)		
$TiO(\eta^2\text{-}N_2)_2$ ($^1A_1$)	0.0	1017.8 (154)	1979.1 (140)	2043.0 (259)	
$TiO(\eta^1\text{-}NN)_2$ (^{3}A″)	0.9	995.3 (266)	2145.9 (444)	2189.2 (2100)	
$TiO(\eta^1\text{-}NN)_3$ ($^3A_1$)	0.0	1004.1 (212)	2194.5 (1225)	2236.8 (154)	
$TiO(\eta^2\text{-}N_2)(\eta^1\text{-}NN)_2$ (^{1}A)	3.5	996.3 (133)	1863.5 (1508)	2191.2 (870)	2244.2 (553)
$TiO(\eta^2\text{-}N_2)(\eta^1\text{-}NN)_2$ (^{3}A″)	3.6	1000.8 (220)	1951.1 (1390)	2158.0 (1692)	2220.6 (593)
$TiO(\eta^2\text{-}N_2)_2(\eta^1\text{-}NN)$ (^{1}A′)	6.2	1007.1 (124)	1932.4 (466)	2063.0 (34)	2208.2 (223)
$TiO(\eta^2\text{-}N_2)_2(\eta^1\text{-}NN)$ (^{3}A″)	7.6	1017.1 (167)	1987.2 (354)	2029.5 (356)	2334.2 (101)
$TiO(\eta^1\text{-}NN)_4$ ($^1A_1$)		993.3 (118)	2117.9 (0)	2134.1 (2573)	2248.5 (57)

Table 3. Relative Energy (kcal/mol), Harmonic Vibrational Frequencies (cm^{-1}), and Intensities (in Parentheses in km/mol) of the $TiO(N_2)_x$ ($x = 1-4$) Complexes Calculated at the B3LYP/6-311+G(d) Level

	relative energy	ν_{TiO}	ν_{NN}	ν_{NN}	ν_{NN}
N_2			2444.9		
TiO ($^3\Delta$)		1042.6 (220)			
TiO(η^1-NN) (^{3}A″)	0.0	1019.0 (289)	2197.4 (1946)		
TiO(η^2-N_2) ($^1A_1$)	2.0	1028.8 (256)	1795.7 (348)		
$TiO(\eta^2\text{-}N_2)_2$ ($^1A_1$)	0.0	1045.6 (258)	1958.6 (1832)	2043.8 (111)	
$TiO(\eta^1\text{-}NN)_2$ (^{3}A″)	−2.1	1007.9 (328)	2071.9 (3383)	2163.8 (290)	
$TiO(\eta^1\text{-}NN)_3$ ($^3A_1$)	0.0	1008.8 (296)	2142.9 (1920)	2246.4 (130)	
$TiO(\eta^2\text{-}N_2)(\eta^1\text{-}NN)_2$ (^{1}A)	4.4	1026.0 (216)	1982.3 (1296)	2246.4 (884)	2302.9 (403)
$TiO(\eta^2\text{-}N_2)(\eta^1\text{-}NN)_2$ (^{3}A″)	4.9	1018.1 (277)	2018.6 (972)	2197.2 (1479)	2270.2 (345)
$TiO(\eta^2\text{-}N_2)_2(\eta^1\text{-}NN)$ (^{1}A′)	8.8	1038.1 (261)	2073.3 (1681)	2109.5 (258)	2314.9 (306)
$TiO(\eta^2\text{-}N_2)_2(\eta^1\text{-}NN)$ (^{3}A″)	10.9	1030.1 (261)	2027.0 (1101)	2073.3 (466)	2333.3 (334)
$TiO(\eta^1\text{-}NN)_4$ ($^1A_1$)		1017.7 (205)	2215.2 (0)	2230.3 (1815)	2318.4 (51)

equivalent end-on bonded N_2 ligands. The structures with one or two side-on bonded N_2 ligands lie more than 3 kcal/mol higher in energy (Tables 2 and 3). The C_{3v} structure was predicted to have one strong doubly degenerate N−N stretching mode at 2194.5 (mPW2PLYP) and 2142.9 cm^{-1} (B3LYP). Experimentally, two absorptions with almost the same IR intensities were observed. These two absorptions could either be due to different sites of the doubly degenerate mode of the C_{3v} complex or be due to two different modes for a distorted complex. Different sites are quite unlikely since the relative intensities of these two absorptions remain constant in all experiments. Therefore, these two absorptions are probably due to two modes for a distorted complex. Similar distortions in solid matrixes have been observed for some high-symmetry molecules.[41]

$TiO(\eta^1\text{-}NN)_4$. The absorptions at 2084.0 and 960.2 cm^{-1} are attributed to $TiO(\eta^1\text{-}NN)_4$. These absorptions markedly increased on annealing and are favored with relatively high N_2 concentrations. The upper absorption is due to a N−N stretching vibration, which dominated the spectrum in the N−N stretching frequency region after high temperature annealing. At least three intermediate absorptions at 2056.0, 2040.7, and 2024.9 cm^{-1} can clearly be resolved in the experiment with the mixed $^{14}N_2 + {}^{15}N_2$ sample (Figure 3). The isotopic structure in the experiment with scrambled $^{14}N_2 + {}^{14}N^{15}N + {}^{15}N_2$ sample is too weak to be resolved due to isotopic dilution. The 960.2 cm^{-1} absorption showed no shift with $^{15}N_2$ and is appropriate for a Ti═O stretching mode, which is about 37.7 cm^{-1} red-shifted from that of TiO.

The $TiO(\eta^1\text{-}NN)_4$ complex was predicted to have a $^1A_1$ ground state with C_{4v} symmetry with four N_2 ligands end-on bonded to the titanium metal center (Figure 7). The Ti═O bond was predicted to be 1.632 Å, lengthened by 0.02 Å upon four N_2 coordination. As listed in Table 3, there are three N−N stretching vibrational modes for the C_{4v} symmetry $TiO(\eta^1\text{-}NN)_4$ complex. The doubly degenerate antisymmetric stretching mode was predicted to have the largest IR intensity (Tables 2 and 3). The other two modes are either IR inactive (b_2 mode) or has very small IR intensity (a_1 mode, about 50 km/mol). The calculated isotopic splittings also fit the mixed $^{14}N_2 + {}^{15}N_2$ spectrum, and lend additional support to the assignment.

$TiO_2(\eta^1\text{-}NN)_x$ ($x = 1-4$). Weak absorptions at 925.5, 915.8, 906.8, and 901.0 cm^{-1} were produced on sample annealing to different temperatures (Figure 2). These absorptions exhibited no shift with $^{15}N_2$. The band positions suggest that these absorptions are due to antisymmetric TiO_2 stretching vibrations of the TiO_2 $(\eta^1\text{-}NN)_x$ complexes (Table 1). A much weak absorption at 955.2 cm^{-1} tracked with the 925.5 cm^{-1} absorption and is attributed to the symmetric TiO_2 stretching mode of the $TiO_2(\eta^1\text{-}NN)$ complex.

dx.doi.org/10.1021/jp203352e |J. Phys. Chem. A 2011, 115, 6551–6558

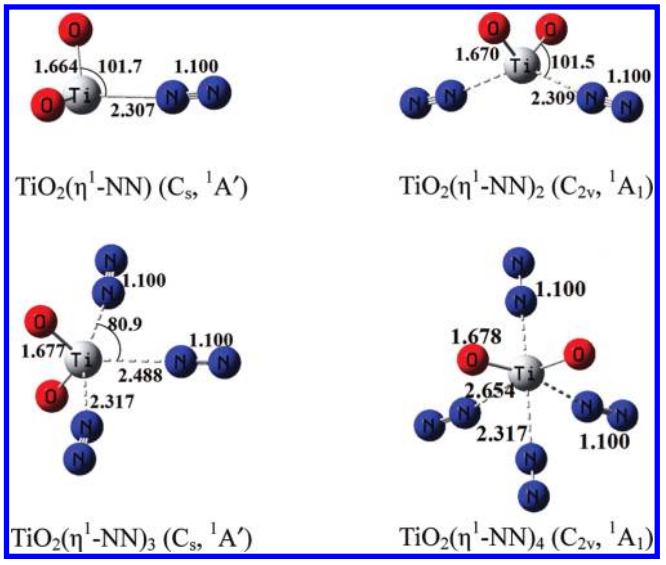

Figure 8. Structures (bond lengths in Å and bond angles in degrees) of the $TiO_2(\eta^1\text{-NN})_x$ (x = 1−4) complexes optimized at the mPW2PLYP/6-311+G(d) level.

The symmetric TiO_2 stretching modes of the other complexes were not observed either due to weakness or being overlapped by the strong TiO_2 absorptions. No obvious absorptions were observed in the N−N stretching frequency region, suggesting that the N−N stretching modes of these complexes are too weak to be observed. Theoretical calculations predicted that TiO_2 is able to coordinate up to four N_2 molecules in forming the $TiO_2(\eta^1\text{-NN})_x$ (x = 1−4) complexes with end-on bonded N_2 ligands (Figure 8). The calculated total binding energy increases monotonically with increasing N_2 coordination (Table 4). The calculated TiO_2 stretching frequencies of the $TiO_2(\eta^1\text{-NN})_x$ (x = 1−4) series exhibit a monotonic red-shift upon successive N_2 coordination (Table 5). As listed in Table 5, all of the N−N stretching vibrations of the $TiO_2(\eta^1\text{-NN})_x$ (x = 1−4) complexes have very low IR intensities and cannot be observed experimentally.

The $^3A''$ ground state $TiO(\eta^1\text{-NN})$ complex can be viewed as being formed by the interaction of the ground state TiO and N_2. The TiO molecule has a $^3\Delta$ ground state with an electron configuration of $(\text{core})(\sigma)^1(\delta)^1$. The singly occupied σ orbital is primarily a hybrid of the Ti 4s, $4p_z$, and $3d_z^2$ orbitals that is polarized away from the O atom. The singly occupied δ orbital is largely the Ti 3d orbital that is mainly nonbonding. The interactions between TiO and N_2 are dominated by the synergic donations of filled orbitals of N_2 into an empty σ-symmetry acceptor orbital of TiO, a hybrid orbital of the Ti 4s, $4p_z$, and $3d_z^2$ orbitals and the back-donation of the TiO electrons to the empty π^* orbitals of N_2. Because the σ orbital is singly occupied, the donation interaction is weak due to σ repulsion. The singly occupied δ molecular orbital of TiO is the back-donation orbital. It interacts with the π^* antibonding orbitals of N_2 in the end-on fashion, which favors a structure with the TiO bond perpendicular to the TiNN plane. The optimized structure of $TiO(\eta^1\text{-NN})$ has an OTiN bond angle of 96.9°, very close to 90°. The binding energy with respect to TiO ($^3\Delta$) + N_2 was estimated to be 5.5 and 1.6 kcal/mol at the B3LYP and mPW2PLYP levels of theory after zero point energy corrections.

Table 4. Calculated Binding Energies (Kcal/mol) of the $TiO_{1-2}(N_2)_x$ (x = 1−4) Complexes with Respect to TiO ($^3\Delta$) + xN_2 and TiO_2 ($^1A_1$) + xN_2 at 0 K after Zero Point Energy Correction

	B3LYP	mPW2PLYP
$TiO(\eta^1\text{-NN})$ (C_s, $^3A''$)	5.5	1.6
$TiO(\eta^2\text{-N}_2)$ (C_s, $^1A'$)	3.5	1.1
$TiO(\eta^2\text{-N}_2)_2$ (C_{2v}, $^1A_1$)	18.6	11.9
$TiO(\eta^1\text{-N}_2)_2$ (C_s, $^3A''$)	20.6	11.0
$TiO(\eta^1\text{-NN})_3$ (C_{3v}, $^3A_1$)	37.9	29.5
$TiO(\eta^2\text{-N}_2)(\eta^1\text{-NN})_2$ (C_1, ^1A)	33.5	25.9
$TiO(\eta^2\text{-N}_2)(\eta^1\text{-NN})_2$ (C_s, $^3A''$)	33.0	25.9
$TiO(\eta^2\text{-N}_2)_2(\eta^1\text{-NN})$ (C_s, $^1A'$)	27.0	23.2
$TiO(\eta^2\text{-N}_2)_2(\eta^1\text{-NN})$ (C_s, $^3A''$)	27.0	21.9
$TiO(\eta^1\text{-NN})_4$ (C_{4v}, $^1A_1$)	49.6	46.5
$TiO_2(\eta^1\text{-NN})$ (C_s, $^1A'$)	10.7	11.9
$TiO_2(\eta^1\text{-NN})_2$ (C_{2v}, $^1A_1$)	21.3	23.9
$TiO_2(\eta^1\text{-NN})_3$ (C_s, $^1A'$)	25.4	30.0
$TiO_2(\eta^1\text{-NN})_4$ (C_{2v}, $^1A_1$)	26.4	33.1

The $^1A_1$ ground state $TiO(\eta^2\text{-N}_2)_2$ and $TiO(\eta^1\text{-NN})_4$ complexes can be viewed as being formed by the interaction of an singlet excited state TiO fragment with the N_2 ligands. The singlet excited state TiO has an electron configuration of $(\text{core})(\delta)^2(\sigma)^0$. Upon excitation, the σ orbital is empty and is able to accept σ donation from N_2. The δ orbital which is largely the Ti 3d orbital that is oriented in the plane perpendicular to the TiO bond is doubly occupied and acts as an orbital for back-donation from TiO to N_2. Therefore, both the $TiO(\eta^2\text{-N}_2)_2$ and $TiO(\eta^1\text{-NN})_4$ complexes are more strongly bound than $TiO(\eta^1\text{-NN})$ due to increased σ donation and π backdonation. As listed in Table 4, the binding energies per N_2 in $TiO(\eta^2\text{-N}_2)_2$ and $TiO(\eta^1\text{-NN})_4$ are larger than that of $TiO(\eta^1\text{-NN})$.

The infrared spectra shown in Figures 1 and 2 clearly demonstrate that the titanium oxide molecules reacted with dinitrogen to form the $TiO(N_2)_x$ and $TiO_2(\eta^1\text{-NN})_x$ (x = 1−4) complexes, reactions 1−8. These reactions proceeded via the ground state titanium oxide molecules in solid neon upon annealing. The spontaneous formation of these dinitrogen complexes upon sample annealing implies that negligible activation energy is required for these addition reactions. According to density functional calculations at the B3LYP/6-311+G(d) level, the stepwise formation of the complexes is energetically favored:

$$\text{TiO}(^3\Delta) + \text{N}_2(^1\Sigma_g) \rightarrow \text{TiO}(\eta^1 - \text{NN})(^3\text{A}'') \qquad \Delta E = -5.5 \text{ kcal/mol} \quad (1)$$

$$\text{TiO}(\eta^1 - \text{NN})(^3\text{A}'') + \text{N}_2(^1\Sigma_g) \rightarrow \text{TiO}(\eta^2 - \text{N}_2)_2(^1\text{A}_1) \qquad \Delta E = -13.1 \text{ kcal/mol} \quad (2)$$

$$\text{TiO}(\eta^2 - \text{N}_2)_2(^1\text{A}_1) + \text{N}_2(^1\Sigma_g) \rightarrow \text{TiO}(\eta^1 - \text{NN})_3(^3\text{A}_1) \qquad \Delta E = -19.3 \text{ kcal/mol} \quad (3)$$

$$\text{TiO}(\eta^1 - \text{NN})_3(^3\text{A}_1) + \text{N}_2(^1\Sigma_g) \rightarrow \text{TiO}(\eta^1 - \text{NN})_4(^1\text{A}_1) \qquad \Delta E = -11.7 \text{ kcal/mol} \quad (4)$$

dx.doi.org/10.1021/jp203352e |J. Phys. Chem. A 2011, 115, 6551–6558

Table 5. Harmonic Vibrational Frequencies (cm^{-1}) and Intensities (in Parentheses in km/mol) of the $TiO_2(\eta^1\text{-NN})_x$ ($x = 1-4$) Complexes Calculated at the mPW2PLYP/6-311+G(d) and B3LYP/6-311+G(d) Levels

	ν_{TiO}	ν_{TiO}	ν_{NN}	ν_{NN}	ν_{NN}	
			mPW2PLYP			
TiO_2 ($^1A_1$)	944.2 (357)	952.1 (21)				
$TiO_2(\eta^1\text{-NN})$ (C_s, $^1A'$)	932.4 (322)	944.2 (21)	2386.0 (1)			
$TiO_2(\eta^1\text{-NN})_2$ (C_{2v}, $^1A_1$)	920.4 (288)	936.1 (21)	2384.9 (0)	2385.2 (3)		
$TiO_2(\eta^1\text{-NN})_3$ (C_s, $^1A'$)	910.6 (286)	925.0 (25)	2381.2 (2)	2381.6 (5)	2383.7 (1)	
$TiO_2(\eta^1\text{-NN})_4$ (C_{2v}, $^1A_1$)	908.3 (339)	920.8 (34)	2376.0 (2)	2376.6 (0)	2381.1 (1)	2381.5 (5)
			B3LYP			
TiO_2 ($^1A_1$)	978.8 (470)	1026.0 (39)				
$TiO_2(\eta^1\text{-NN})$ (C_s, $^1A'$)	961.6 (416)	1013.0 (40)	2446.7 (6)			
$TiO_2(\eta^1\text{-NN})_2$ (C_{2v}, $^1A_1$)	945.7 (368)	1000.7 (39)	2445.2 (6)	2446.6 (9)		
$TiO_2(\eta^1\text{-NN})_3$ (C_s, $^1A'$)	931.9 (352)	986.8 (42)	2441.5 (16)	2442.8 (8)	2452.8 (0)	
$TiO_2(\eta^1\text{-NN})_4$ (C_{2v}, $^1A_1$)	926.6 (412)	982.5 (51)	2442.7 (15)	2443.6 (3)	2444.4 (1)	2445.9 (7)

$$TiO_2(^1A_1) + N_2(^1\Sigma_g) \rightarrow TiO_2(\eta^1 - NN)(^1A') \quad \Delta E = -10.7 \text{ kcal/mol} \quad (5)$$

$$TiO_2(\eta^1 - NN)(^1A') + N_2(^1\Sigma_g) \rightarrow TiO_2(\eta^1 - NN)_2(^1A_1) \quad \Delta E = -10.6 \text{ kcal/mol} \quad (6)$$

$$TiO_2(\eta^1 - NN)_2(^1A_1) + N_2(^1\Sigma_g) \rightarrow TiO_2(\eta^1 - NN)_3(^1A') \quad \Delta E = -4.1 \text{ kcal/mol} \quad (7)$$

$$TiO_2(\eta^1 - NN)_3(^1A') + N_2(^1\Sigma_g) \rightarrow TiO_2(\eta^1 - NN)_4(^1A_1) \quad \Delta E = -1.0 \text{ kcal/mol} \quad (8)$$

Upon the formation of the $TiO(N_2)_x$ complexes, dinitrogen is activated where the N−N bond is elongated by 0.014, 0.048, 0.018, and 0.014 Å in the $TiO(\eta^1\text{-NN})$, $TiO(\eta^2\text{-}N_2)_2$, $TiO(\eta^1\text{-NN})_3$, and $TiO(\eta^1\text{-NN})_4$ complexes, respectively, at the B3LYP/6-311+G(d) level. Wiberg bond order analysis indicates that the N−N bond order is reduced by 0.24, 0.52, 0.29, and 0.24, respectively, in the four complexes, respectively.[42] The N_2 ligands of the $TiO_2(\eta^1\text{-NN})_x$ ($x = 1-4$) complexes are much less activated. The results indicate that TiO has the potential to activate dinitrogen by backdonation of its 3d electrons to the antibonding orbitals of dinitrogen.

CONCLUSIONS

Titanium oxide−dinitrogen complexes have been prepared and characterized using matrix isolation infrared absorption spectroscopy and theoretical calculations. The complexes were prepared by the reactions of titanium oxide molecules with dinitrogen in solid neon. The results show that the titanium monoxide and dioxide molecules are able to coordinate up to four N_2 ligands in forming the $TiO(N_2)_x$ and $TiO_2(\eta^1\text{-NN})_x$ ($x = 1-4$) complexes spontaneously on annealing. The $TiO(\eta^1\text{-NN})$ complex is end-on bonded and was predicted to have a $^3A''$ ground state arising from the $^3\Delta$ ground state of TiO. Argon doping experiments indicate that $TiO(\eta^1\text{-NN})$ is able to coordinate argon atom(s) in forming complex. Argon atom coordination induces a large red-shift of the N−N stretching frequency. The $TiO(\eta^2\text{-}N_2)_2$ complex was characterized to have a C_{2v} symmetry, in which both the N_2 ligands are side-on bonded to the titanium metal center. The $TiO(\eta^1\text{-NN})_3$ and $TiO(\eta^1\text{-NN})_4$ complexes are end-on bonded. The $TiO(\eta^2\text{-}N_2)_2$ and $TiO(\eta^1\text{-NN})_4$ complexes were predicted to have singlet ground states arising from an excited state of TiO, and are more strongly bound than the $TiO(\eta^1\text{-NN})$ complex. The $TiO_2(\eta^1\text{-NN})_x$ ($x = 1-4$) complexes were predicted to be end-on bonded.

AUTHOR INFORMATION

Corresponding Author

*E-mail: mfzhou@fudan.edu.cn; lizhenhua@fudan.edu.cn.

ACKNOWLEDGMENT

We gratefully acknowledge financial support from the National Natural Science Foundation of China (Grant No. 20933003) and National Basic Research Program of China (2007CB815203, 2009CB623506, 2011CB808505, and 2010CB732306).

REFERENCES

(1) (a) Howard, J. B.; Rees, D. C. *Chem. Rev.* **1996**, *96*, 2965. (b) Burgess, B. K.; Lowe, D. J. *Chem. Rev.* **1996**, *96*, 2983. (c) Schlogl, R. *Angew. Chem., Int. Ed.* **2003**, *42*, 2004.
(2) Allen, A. D.; Senoff, C. V. *Chem. Commun.* **1965**, 621.
(3) (a) Hidai, M.; Mizobe, Y. *Chem. Rev.* **1995**, *95*, 1115. (b) Hidai, M. *Coord. Chem. Rev.* **1999**, *185−186*, 99.
(4) Richards, R. L. *Coord. Chem. Rev.* **1996**, *154*, 83.
(5) Hazari, N. *Chem. Soc. Rev.* **2010**, *39*, 4044.
(6) (a) Fryzuk, M. D. *Acc. Chem. Res.* **2009**, *42*, 127. (b) Ohki, Y.; Fryzuk, M. D. *Angew. Chem., Int. Ed.* **2007**, *46*, 3180. (C) Fryzuk, M. D.; Johnson, S. A. *Coord. Chem. Rev.* **2000**, *200*, 379.
(7) Crossland, J. L.; Tyler, D. R. *Coord. Chem. Rev.* **2010**, *254*, 1883.
(8) Schrock, R. R. *Angew. Chem., Int. Ed.* **2008**, *47*, 5512.
(9) Nikiforov, G. B.; Vidyaratne, I.; Gambarotta, S.; Korobkov, I. *Angew. Chem., Int. Ed.* **2009**, *48*, 7415.
(10) Himmel, H. J.; Reiher, M. *Angew. Chem., Int. Ed.* **2006**, *45*, 6264.
(11) (a) Chertihin, G. V.; Andrews, L.; Bauschlicher, C. W., Jr. *J. Am. Chem. Soc.* **1998**, *120*, 3205. (b) Chertihin, G. V.; Bare, W. D.; Andrews, L. *J. Phys. Chem. A* **1998**, *102*, 3697.
(12) Kushto, G. P.; Souter, P. F.; Chertihin, G. V.; Andrews, L. *J. Chem. Phys.* **1999**, *110*, 9020.
(13) Zhou, M. F.; Andrews, L. *J. Phys. Chem. A* **1998**, *102*, 9061.
(14) Andrews, L.; Bare, W. D.; Chertihin, G. V. *J. Phys. Chem. A* **1997**, *101*, 8417.

(15) Chertihin, G. V.; Andrews, L.; Neurock, M. *J. Phys. Chem.* **1996**, *100*, 14609.
(16) (a) Andrews, L.; Citra, A.; Chertihin, G. V.; Bare, W. D.; Neurock, M. *J. Phys. Chem. A* **1998**, *102*, 2561. (b) Wang, X. F.; Andrews, L. *J. Phys. Chem. A* **2002**, *106*, 2457. (c) Citra, A.; Wang, X. F.; Bare, W. D.; Andrews, L. *J. Phys. Chem. A* **2001**, *105*, 7799.
(17) (a) Lu, Z. H.; Jiang, L.; Xu, Q. *J. Phys. Chem. A* **2010**, *114*, 2157. (b) Lu, Z. H.; Jiang, L.; Xu, Q. *J. Chem. Phys.* **2009**, *131*, 034512.
(18) Elustondo, F.; Mascetti, J.; Papai, I. *J. Phys. Chem. A* **2000**, *104*, 3572.
(19) Souvi, S. M.; Tremblay, B.; Perchard, J. P.; Alikhani, M. E. *J. Chem. Phys.* **2009**, *130*, 074304.
(20) Himmel, H. J.; Hubner, O.; Klopper, W.; Manceron, L. *Angew. Chem., Int. Ed.* **2006**, *45*, 2799.
(21) Gong, Y.; Zhao, Y. Y.; Zhou, M. F. *J. Phys. Chem. A* **2007**, *111*, 6204.
(22) Zhou, M. F.; Jin, X.; Gong, Y.; Li, J. *Angew. Chem., Int. Ed.* **2007**, *46*, 2911.
(23) Zhou, M. F.; Zhang, L. N.; Qin, Q. Z. *J. Phys. Chem. A* **2001**, *105*, 6407.
(24) Chen, M. H.; Wang, G. J.; Jiang, G. Y.; Zhou, M. F. *J. Phys. Chem. A* **2005**, *109*, 415.
(25) Zhou, M. F.; Wang, G. J.; Zhao, Y. Y.; Chen, M. H.; Ding, C. F. *J. Phys. Chem. A* **2005**, *109*, 5079.
(26) Chen, M. H.; Wang, G. J.; Zhou, M. F. *Chem. Phys. Lett.* **2005**, *409*, 70.
(27) Wang, C. X.; Zhuang, J.; Wang, G. J.; Chen, M. H.; Zhao, Y. Y.; Zheng, X. M.; Zhou, M. F. *J. Phys. Chem. A* **2010**, *114*, 8083.
(28) Lu, Z. H.; Xu, Q. *Chem. Phys. Lett.* **2011**, *503*, 33.
(29) (a) Zhao, Y. Y.; Wang, G. J.; Chen, M. H.; Zhou, M. F. *J. Phys. Chem. A* **2005**, *109*, 6621. (b) Zhao, Y. Y.; Gong, Y.; Chen, M. H.; Ding, C. F.; Zhou, M. F. *J. Phys. Chem. A* **2005**, *109*, 11765. (c) Zhao, Y. Y.; Gong, Y.; Zhou, M. F. *J. Phys. Chem. A* **2006**, *110*, 10777.
(30) (a) Zhao, Y. Y.; Gong, Y.; Chen, M. H.; Zhou, M. F. *J. Phys. Chem. A* **2006**, *110*, 1845. (b) Zhao, Y. Y.; Zheng, X. M.; Zhou, M. F. *Chem. Phys.* **2008**, *351*, 18.
(31) (a) Wang, G. J.; Zhou, M. F. *Int. Rev. Phys. Chem.* **2008**, *27*, 1. (b) Zhou, M. F.; Andrews, L.; Bauschlicher, C. W., Jr. *Chem. Rev.* **2001**, *101*, 1931.
(32) (a) Becke, A. D. *J. Chem. Phys.* **1993**, *98*, 5648. (b) Lee, C.; Yang, W.; Parr, R. G. *Phys. Rev. B* **1988**, *37*, 785.
(33) Schwabe, T.; Grimme, S. *Phys. Chem. Chem. Phys.* **2006**, *8*, 438.
(34) (a) McLean, A. D.; Chandler, G. S. *J. Chem. Phys.* **1980**, *72*, 5639. (b) Krishnan, R.; Binkley, J. S.; Seeger, R.; Pople, J. A. *J. Chem. Phys.* **1980**, *72*, 650.
(35) (a) Cramer, C. J.; Truhlar, D. G. *Phys. Chem. Chem. Phys.* **2009**, *11*, 10757. (B) Sousa, S. F.; Fernandes, P. A.; Ramos, M. J. *J. Phys. Chem. A* **2007**, *111*, 10439.
(36) Goerigk, L.; Grimme, S. *J. Chem. Theory Comput.* **2011**, *7*, 291.
(37) Peng, C.; Ayala, P. Y.; Schlegel, H. B.; Frisch, M. J. *J. Comput. Chem.* **1996**, *17*, 49.
(38) Frisch, M. J.; Trucks, G. W.; Schlegel, H. B.; Scuseria, G. E.; Robb, M. A.; Cheeseman, J. R.; Scalmani, G.; Barone, V.; Mennucci, B.; Petersson, G. A.; Nakatsuji, H.; Caricato, M.; Li, X.; Hratchian, H. P.; Izmaylov, A. F.; Bloino, J.; Zheng, G.; Sonnenberg, J. L.; Hada, M.; Ehara, M.; Toyota, K.; Fukuda, R.; Hasegawa, J.; Ishida, M.; Nakajima, T.; Honda, Y.; Kitao, O.; Nakai, H.; Vreven, T.; Montgomery, J. A., Jr.; Peralta, J. E.; Ogliaro, F.; Bearpark, M.; Heyd, J. J.; Brothers, E.; Kudin, K. N.; Staroverov, V. N.; Kobayashi, R.; Normand, J.; Raghavachari, K.; Rendell, A.; Burant, J. C.; Iyengar, S. S.; Tomasi, J.; Cossi, M.; Rega, N.; Millam, J. M.; Klene, M.; Knox, J. E.; Cross, J. B.; Bakken, V.; Adamo, C.; Jaramillo, J.; Gomperts, R.; Stratmann, R. E.; Yazyev, O.; Austin, A. J.; Cammi, R.; Pomelli, C.; Ochterski, J. W.; Martin, R. L.; Morokuma, K.; Zakrzewski, V. G.; Voth, G. A.; Salvador, P.; Dannenberg, J. J.; Dapprich, S.; Daniels, A. D.; Farkas, O.; Foresman, J. B.; Ortiz, J. V.; Cioslowski, J.; , Fox, D. J. *Gaussian 09*, Revision A.02, Gaussian, Inc.: Wallingford, CT, 2009.
(39) (a) Chertihin, G. V.; Andrews, L. *J. Phys. Chem.* **1995**, *99*, 6356. (b) Gong, Y.; Zhou, M. F.; Andrews, L. *Chem. Rev.* **2009**, *109*, 6765.
(40) (a) Gong, Y.; Zhou, M. F.; Tian, S. X.; Yang, J. L. *J. Phys. Chem. A* **2007**, *111*, 6127. (b) Gong, Y.; Zhou, M. F. *J. Phys. Chem. A* **2008**, *112*, 9758. (c) Gong, Y.; Zhang, Q. Q.; Zhou, M. F. *J. Phys. Chem. A* **2007**, *111*, 3534.
(41) (a) Zhou, M. F.; Andrews, L. *J. Phys. Chem. A* **2000**, *104*, 1648. (b) Poliakoff, M.; Turner, J. J. *J. Chem. Soc. A* **1971**, 654.
(42) Wiberg, K. A. *Tetrahedron* **1968**, *24*, 1083.